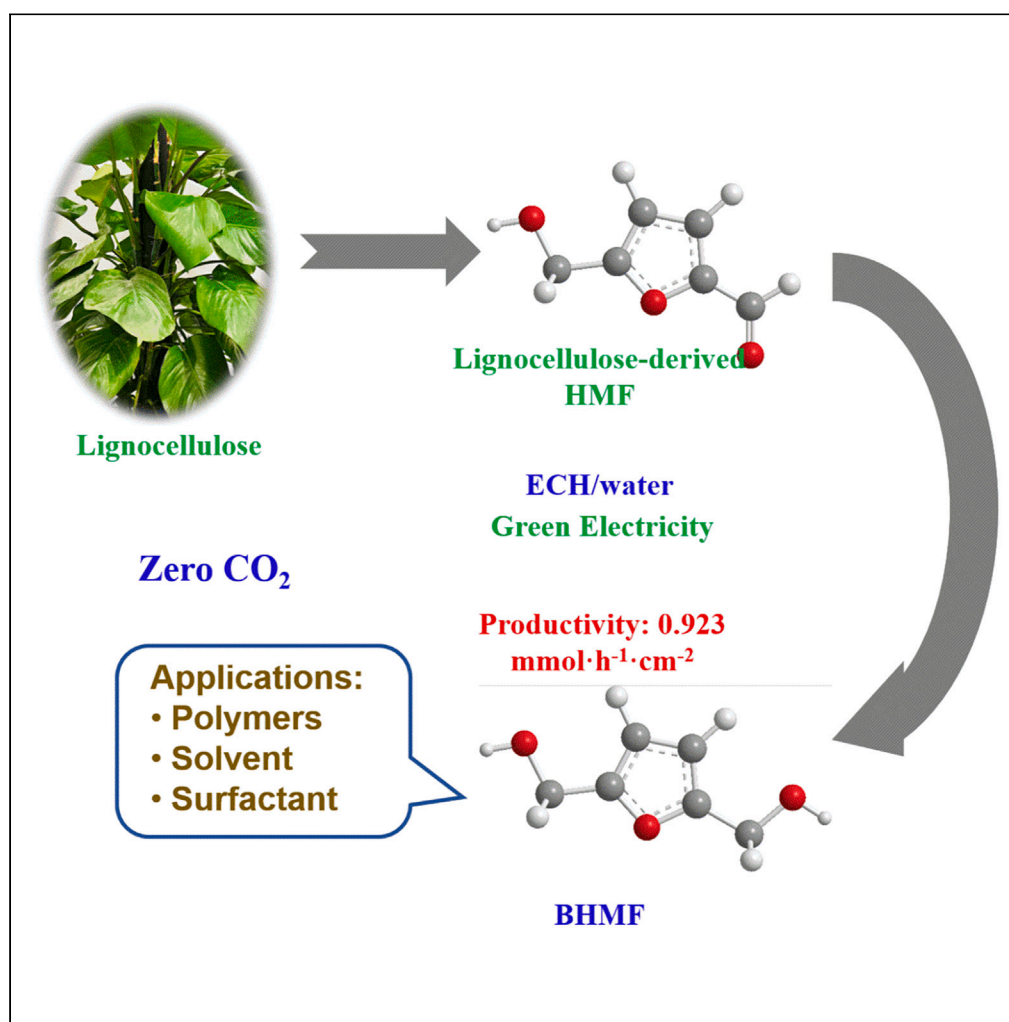


## Article

## Selective electrocatalytic hydrogenation of lignocellulose-derived 5-hydroxymethylfurfural with superior productivities



Dingyi Zhang,  
Guanwu Lian,  
Wenbin Zhang, ...,  
Baiyao Liang, Yun  
Zhang, Wei Zhao

weizhao@szu.edu.cn

**Highlights**

An efficient ECH system is developed for valorization of HMF

High productivity has been achieved at a current density of 100 mA cm<sup>-2</sup>

High selectivity (97%) and FE (72%) have been achieved at 50 mA cm<sup>-2</sup> current density

The stability of the electrocatalysis system is outstanding

Zhang et al., iScience 26,  
108003  
October 20, 2023 © 2023 The  
Author(s).  
[https://doi.org/10.1016/  
j.isci.2023.108003](https://doi.org/10.1016/j.isci.2023.108003)

## Article

## Selective electrocatalytic hydrogenation of lignocellulose-derived 5-hydroxymethylfurfural with superior productivities

Dingyi Zhang,<sup>1,2</sup> Guanwu Lian,<sup>1,2</sup> Wenbin Zhang,<sup>1,2</sup> Zhousheng Mo,<sup>1</sup> Henan Chen,<sup>1</sup> Baiyao Liang,<sup>1</sup> Yun Zhang,<sup>1</sup> and Wei Zhao<sup>1,3,\*</sup>

## SUMMARY

Recently, valorization of biomass to value-added chemicals has drawn increasing attention due to carbon neutrality and sustainability. 5-Hydroxymethylfurfural is an important lignocellulose-derived biomass molecule. Herein, we have demonstrated the efficient electrocatalytic hydrogenation of 5-hydroxymethylfurfural to value-added 2,5-bis(hydroxymethyl)furan. An optimized electrolyzer with a highly electrolyte-permeable Pd cathode well balanced the selectivity, faradaic efficiency, and productivity. We have achieved high selectivity (97%) and faradaic efficiency (72%) at 50 mA cm<sup>-2</sup> current density, and a record high productivity of 0.923 mmol cm<sup>-2</sup>·h<sup>-1</sup> at 100 mA cm<sup>-2</sup> current density, ~2 times advanced compared with the best productivity in prior reports. We applied *in situ* infrared reflection-absorption spectroscopy to investigate the electrode-potential-dependent reaction pathways and mechanism, confirming that the highly selective hydrogenation of HMF is due to the tilted adsorption geometry through carbonyl group bonding to the surface of electrode. This work offers an opportunity for the sustainable electrocatalytic valorization of renewable lignocellulose-derived biomass with superior productivities approaching industrial level.

## INTRODUCTION

Biomass resources are the only renewable organic carbon resources in nature, which have extensive sources but remain underutilized. Conversion of biomass provides a promising alternative to fossil feedstocks to produce fuels and valuable chemicals,<sup>1–4</sup> which helps mitigate greenhouse gas (e.g., CO<sub>2</sub>) emission and fulfill the goal of carbon neutrality.<sup>5–7</sup> Each year, more than 40 million tons of inedible plant materials are thrown away, such as wheat stems, corn stover, and wood shavings.<sup>8</sup> It is a huge appeal to converting these discarded plants into lignocellulosic biomass, and then further valorization to high value-added chemicals.<sup>9–11</sup> 5-Hydroxymethylfurfural (HMF) is a widely used organic feedstock in the industry (Figure 1A), which can be derived from lignocellulose.<sup>12–14</sup> HMF is an unsaturated furan ring with hydroxyl group (-OH) and carbonyl group (-C=O), which can be selectively hydrogenated to dialcohols or aldehydes, e.g., 2,5-bis(hydroxymethyl)furan (BHMF), 2,5-bis(hydroxymethyl)tetrahydrofuran, 2-hydroxymethyl-5-methylfuran (HMMF), 5-methylfurfural (MF), and 5,5'-bis(hydroxymethyl)hydrofuroin (BHH) (Figure S1).<sup>12,15</sup> Especially, BHMF is an important pharmaceutical intermediate and industrial feedstock, as solvent, surfactant, and monomer for making functionalized polyethers, polyurethanes, and polyamides.<sup>16,17</sup> Investigation shows that the market prices of HMF and BHMF are \$5 and \$20 per kg, respectively, implying a potential economic value adding for hydrogenation of HMF to BHMF.

Up to now, thermocatalytic hydrogenation (TCH) is mostly studied and applied for the transformation of HMF to BHMF, and noble metal catalysts have been mostly employed.<sup>18–24</sup> However, for the TCH process, high temperature (100°C–150°C) and high pressure (6–65 bar) are required, and “gray hydrogen” gas is used, which causes substantial CO<sub>2</sub> emissions.<sup>25,26</sup>

Alternatively, electrocatalytic hydrogenation (ECH) has been considered as a sustainable route owing to its mild conditions (e.g., room temperature and ambient pressure), especially when powered with green electricity produced by solar and wind energy.<sup>25,27,28</sup> Moreover, ECH utilizes water as the hydrogen source, avoiding the capital cost and complexity of production and transfer of hydrogen gas.<sup>25,26</sup> Previous ECH studies for HMF to BHMF have achieved fairly good faradaic efficiencies (FEs) and selectivity (SE), but with low current densities (<50 mA cm<sup>-2</sup>).<sup>29–32</sup> Very recently, Prof. Duan’s group used a Ru<sub>1</sub>Cu single-atom alloy catalyst for ECH of HMF to BHMF and achieved high FE and SE with a productivity of 0.470 mmol cm<sup>-2</sup>·h<sup>-1</sup> (average current density ≤42 mA cm<sup>-2</sup>).<sup>33</sup> However, for industrially relevant production, larger current densities are needed to achieve higher production efficiency and lower capital costs per unit of productivity.

<sup>1</sup>Institute for Advanced Study, Shenzhen University, Shenzhen, Guangdong 518060, China

<sup>2</sup>These authors contributed equally

<sup>3</sup>Lead contact

\*Correspondence: weizhao@szu.edu.cn

<https://doi.org/10.1016/j.isci.2023.108003>



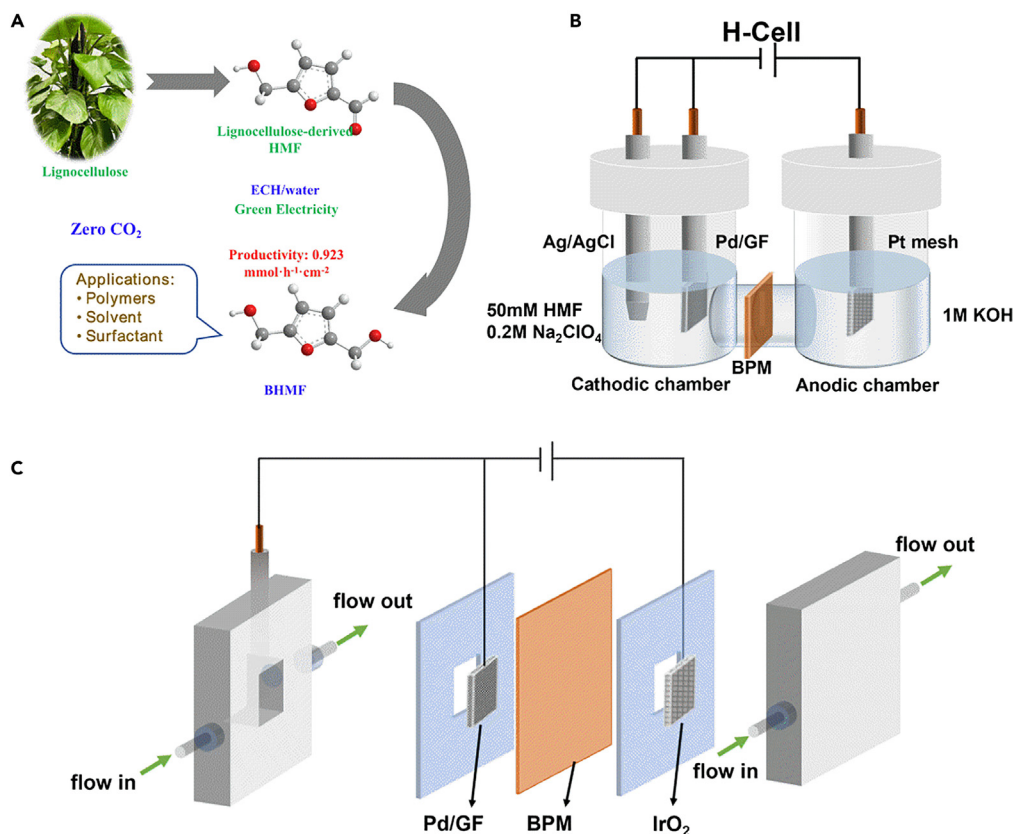


**Figure 1. Scheme of ECH system**

(A) Electrocatalytic hydrogenation of HMF and potential product BHMF.

(B) Schematic illustration of the H-cell system for the ECH of HMF.

(C) Schematic illustration of a flow cell system with a BPM separator. BPM, bipolar membrane.

Herein, we report selective and efficient ECH of HMF toward BHMF with a superior productivity over Pd nanoparticles supported on a graphite felt (GF) as shown in Figure 1B. Our well-optimized ECH system delivers a record-high productivity of 0.923 mmol cm<sup>-2</sup>·h<sup>-1</sup> at a current density of 100 mA cm<sup>-2</sup> (Table S1), which is about twice as high as the best productivity reported previously.<sup>33</sup> High FE (72%) and SE (97%) have been obtained at a current density of 50 mA cm<sup>-2</sup>, comparable to the best prior study.<sup>33</sup> Moreover, *in situ* infrared reflection-absorption spectroscopy (IRRAS) was employed to investigate the mechanism of ECH reaction, revealing that the resulting high SE of BHMF is due to a tilted adsorption geometry of HMF that favors hydrogen attack at the carbonyl group over the furan ring. A techno-economic analysis (TEA) was carefully conducted, and it indicates that our ECH system is feasible for ECH of HMF to BHMF at current densities of 50–100 mA cm<sup>-2</sup>. In contrast to previous studies, our work demonstrates a superior productivity that approaches industrial level, realized by a readily accessible ECH system.

## RESULTS AND DISCUSSION

### Structural characteristic of catalyst

Initially, the architecture of the obtained Pd/GF catalyst was analyzed by scanning electron microscopy (SEM) (Figure S3A). SEM energy dispersive spectrometer analysis suggests a nearly uniform Pd species throughout the GF surface (Figures S3B–S3D). The X-ray photoelectron spectroscopy (XPS) spectrum (Figure S3F) shows the metallic Pd with a slightly oxidized Pd, due to air oxidation, and the oxides were removed by running hydrogen evolution reaction (HER) for 30 min before ECH reaction every time.<sup>34–39</sup> Inductively coupled plasma mass spectroscopy with atomic emission spectrometry indicates 18.63 wt % of Pd on a 1-cm<sup>2</sup> GF (57.4 mg), indicating a Pd loading of 10.69 mg cm<sup>-2</sup>.

X-ray diffraction (XRD) (Figure S4A) depicts a sharp peak of 26.21° and a weak peak of 43.66°, which are, respectively, assigned to the (002) and (100) planes of sp<sup>2</sup>-hybridized graphite carbon.<sup>40,41</sup> The XRD pattern of Pd/GF catalyst exhibits four sharper peaks at 40.16°, 46.70°, 68.17°, and 82.15°, respectively, corresponding to the plane reflections of (111), (200), (220), and (311) crystal planes from metallic palladium (JCPDS No. 46-1043).<sup>42</sup> Transmission electron microscopic (TEM) analysis further confirms random scraped Pd nanoparticles

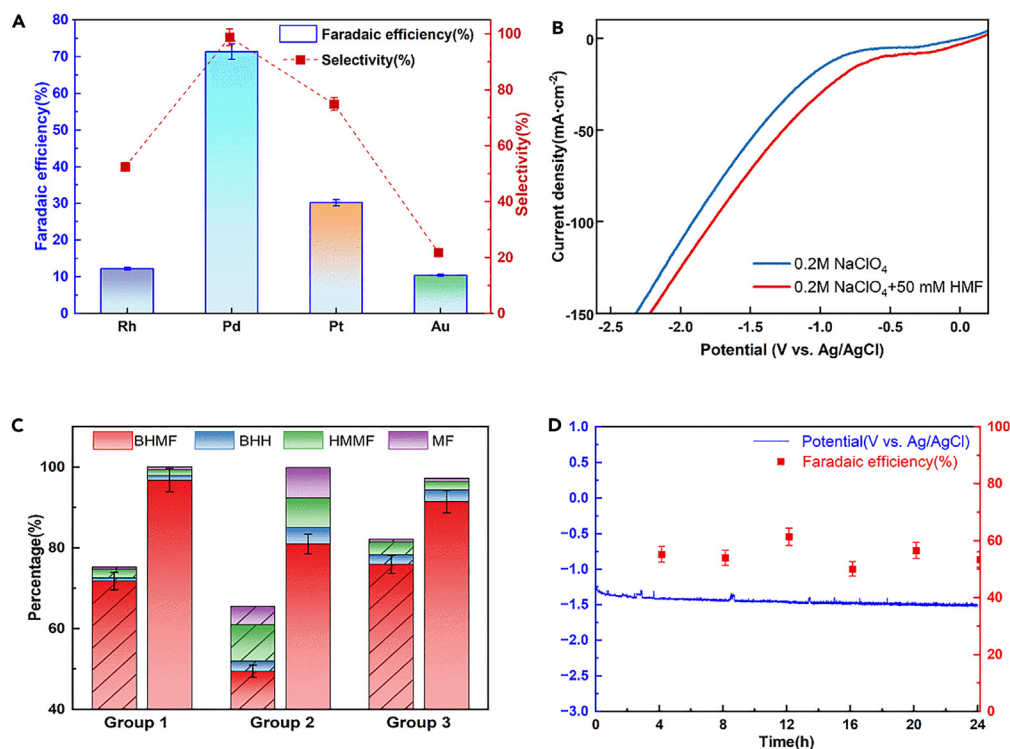


**Figure 2. Screening of catalysts and catalytic results**

(A) FE (blue border columns) and SE of the ECH of HMF over different metal catalysts.

(B) Linear sweep voltammograms curves of Pd/GF in 0.2 M NaClO<sub>4</sub> with or without 50 mM HMF.

(C) FEs (shaded columns) and SEs (bright columns) of each product resulting by the ECH of HMF. Groups 1 and 2 were carried out in an H-cell system at a current density of 50 mA cm<sup>-2</sup> and 100 mA cm<sup>-2</sup>, respectively. Group 3 was carried out in a flow cell system at 50 mA cm<sup>-2</sup>. Columns with diagonal sections suggest FEs, and columns without diagonal sections indicate SEs.

(D) Stable chronopotentiometric operation of Pd/GF at a current density of 50 mA cm<sup>-2</sup> with the optimum FE toward BHMF by using a flow cell system. The error bar is the standard deviation calculated from several experimental data.

from Pd/GF catalyst (Figures S4B and S4C). The image shows crystalline nanoparticles, and the lattice fringes have two interplanar spacings of 2.11 and 1.98 Å, corresponding to the Pd crystal planes of (111) and (200) (JCPDS No. 46-1043), respectively. The cyclic voltammogram diagram (Figure S5) for the underpotential deposition of Cu shows that the electrochemically active surface area (ECSA) of Pd/GF is about 0.76 m<sup>2</sup> g<sup>-1</sup>, which was calculated using the formula  $ECSA = Q_{Cu}/q^s_{Cu}$  and assuming the charge density of a monolayer of Cu requires 407 μC cm<sup>-2</sup>.<sup>43,44</sup>

### Catalytic performance for ECH of HMF

We initially screened catalysts were evaluated for ECH of HMF to BHMF, i.e., Rh, Pt, Pd, and Au nanoparticles supported on GF prepared through the wet-chemical method then by calcination. The cathodic electrolyte was 0.05 M HMF and 0.2 M NaClO<sub>4</sub> (pH 4.52) soluble in pure water, whereas the anodic electrolyte consisted of 1 M KOH solution (Figure 1B). The reaction was performed at 50 mA cm<sup>-2</sup> for 0.5 h. As shown in Figure 2A, the Pd/GF catalyst with 15 mg/mL Pd<sup>2+</sup> loading shows the best FE and SE toward the desired BHMF product from the ECH of HMF when their preparation conditions and the reaction conditions are consistent. Accordingly, the Pd/GF catalyst appears to be a suitable catalyst for ECH of HMF to BHMF. We investigated the electrochemical reduction of HMF with or without HMF in 0.2 M NaClO<sub>4</sub>. Linear sweep voltammograms in Figure 2B show that Pd/GF catalyst exhibits enhanced current density after adding 50 mM HMF, indicating that the ECH of HMF is more preferred and HER is significantly overpressed, evidenced by the FE to BHMF as 72%. ECH of HMF is easier than HER on our Pd/GF catalyst, in terms of lower (more positive) overpotentials, which is also confirmed by IRRAS, where ECH can even occur at positive potentials (vs. reversible hydrogen electrode [RHE]).

The ECH of HMF was performed in a three-electrode H-cell at 50 mA cm<sup>-2</sup> and 100 mA cm<sup>-2</sup> for 0.5 h, and then the solutions were analyzed by high-performance liquid chromatography to identify the ECH products, corresponding to Figure 2C groups 1 and 2, respectively. For group 1, we confirmed a total FE of organic compound of 76%, indicating HER was well suppressed by Pd/GF catalyst. The partial FE for each monomer, i.e., BHMF, BHH, MF, and HMMF, was estimated as 72%, 1%, 1%, and 2.0%, respectively, whereas the SE for BHMF, BHH, MF, and HMMF was estimated to be 97%, 1%, 1%, and 1%, respectively. In addition, the productivity of BHMF at 50 mA cm<sup>-2</sup> was estimated

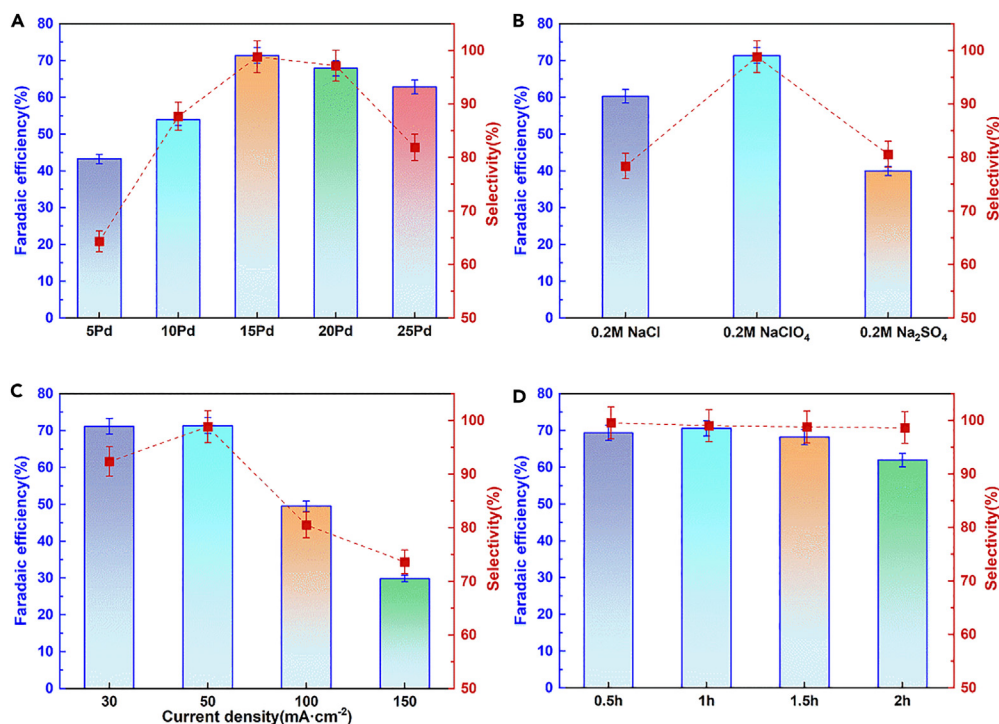


**Figure 3. Catalytic performance tests**

- (A) FE and SE over different loading of Pd<sup>2+</sup> on GF. 5Pd means 5 mg/mL Pd<sup>2+</sup> loading, and so on.  
 (B) FE and SE for ECH of HMF with different electrolytes with the same concentration on 15Pd/GF catalyst.  
 (C) FE and SE at different current densities over the achieved 15Pd/GF catalyst.  
 (D) FE and SE at 50 mA cm<sup>-2</sup> on 15Pd/GF catalyst for a 2-h continuous reaction.

to be 0.669 mmol cm<sup>-2</sup>·h<sup>-1</sup>, superior to any previous report (Table S1). It demonstrated the outstanding capability of our ECH system for HMF to BHMF with a nearly 100% SE and high FE. In contrast to previous studies only running at < 50 mA cm<sup>-2</sup>, we here conducted 100 mA cm<sup>-2</sup> current density, to approach the potential for industrial production with our ECH system. It resulted in 50% FE and 81% SE to target product with a high productivity of 0.923 mmol cm<sup>-2</sup>·h<sup>-1</sup>. The lower but acceptable FE is due to a stronger competing HER. However, more importantly for the industrial-level production, the current density and productivity here have been enhanced by 2-fold compared with previously reported studies for the ECH of HMF (Figure S6; Table S1).

The group 3 in Figure 2C was carried out in a flow cell system (Figure 1C) at 50 mA cm<sup>-2</sup> for 0.5 h, showing a 76% FE and 92% SE toward BHMF. Compared with H-cell at 50 mA cm<sup>-2</sup> for 0.5 h in group 1 in Figure 2C, the FE to BHMF increases (72%–76%) but SE decreases (97%–92%) for the flow cell. We explain it as follows. HER is suppressed in flow cell system more significantly than that in H-cell system, which leads to the increase for the portions of BHMF and other by-products (i.e., BHH, MF). However, the increase of by-products is even a little more than that of BHMF. That is why FE of BHMF increases but SE of BHMF decreases in the way opposite.

We investigated the stability of our ECH system. Initially, we used a flow cell system (Figure 1C and S7B) to duplicate the previous operation at 50 mA cm<sup>-2</sup> over the achieved 15Pd/GF catalyst. Here, we used a flow cell system in a 720 mL solution to perform ECH of HMF instead of the H-cell system because of the limitation of mass transport in the continuous ECH of HMF. FE shows a slight fluctuation during the 24-h continuous ECH of HMF and maintains ~55% toward BHMF at a current density of 50 mA cm<sup>-2</sup> (Figure 2D). And the cathodic potential declines (becomes more negative) a little for 24 h of continuous operation, due to the reduction of reactant concentration in the reaction. Moreover, the characterization of SEM, XPS, and TEM shows the Pd/GF catalyst after the stability test with a negligible change (Figure S8). These results illustrate that our system equipped with the Pd/GF electrode is durable for ECH of HMF to produce BHMF.

To implement high performance for the ECH of HMF, we conducted comparative experiments on the FE and SE of BHMF. We studied the effects of Pd<sup>2+</sup> loading for the ECH of HMF based on the screening of the noble metallic catalysts, and these results are depicted in Figure 3A. Both BHMF FE and SE increased while increasing the Pd<sup>2+</sup> content from 5 to 15 mg/mL. More than 96% of BHMF SE and 72% of BHMF FE were achieved over the Pd/GF catalyst with 15 mg/mL Pd<sup>2+</sup> loading. With a further increase of Pd<sup>2+</sup> loading to 25 mg/mL, the BHMF FE was slightly reduced; however, the SE decreased more significantly. As the Pd<sup>2+</sup> loading increases to a certain extent, the active sites increase and the catalytic performance is enhanced. When the Pd<sup>2+</sup> loading continues to increase, the calcined Pd small particles agglomerate and active sites are reduced, leading to the decline of catalytic performance. Pd/GF with 25 mg/mL catalyst specificity to BHMF was not as high as Pd/GF with 15 mg/mL Pd<sup>2+</sup> loading, and the portions of by-products (e.g., BHH, MF) increased and the amount of BHMF decreased in the reaction. The

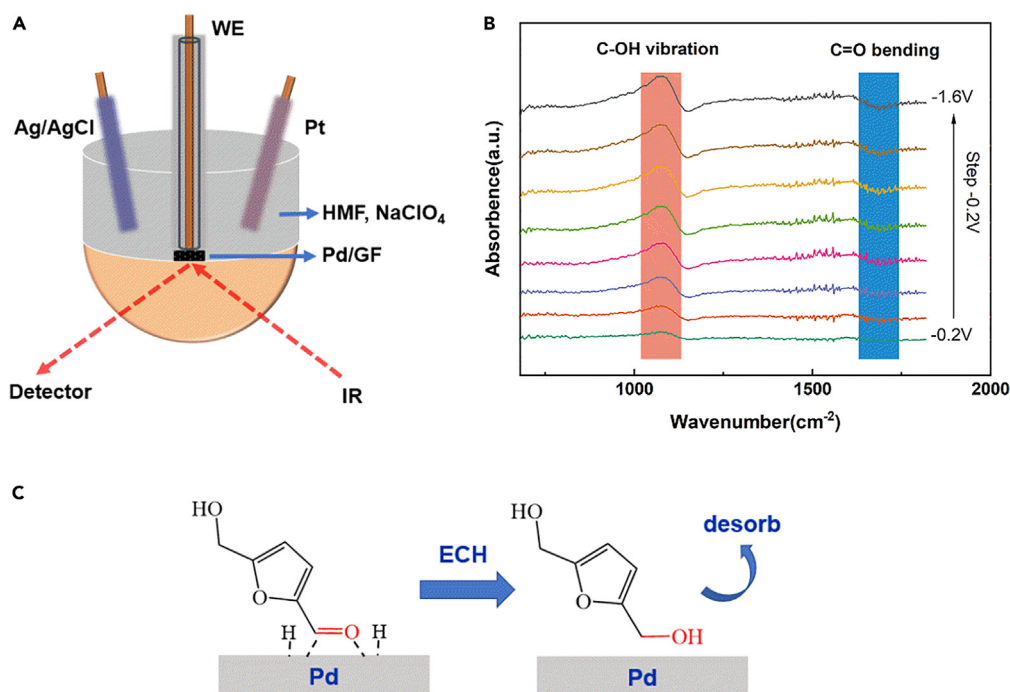


**Figure 4.** *In situ* IRRAS test

(A) *In situ* IRRAS configuration for the ECH of HMF. Pd coated on graphite felt, Ag/AgCl, and Pt mesh as the work, reference, and counter electrode, respectively. (B) *In situ* IRRAS configuration for the ECH of HMF in 0.2 M NaClO<sub>4</sub> electrolyte containing 50 mM HMF in a potential range of  $-0.2$  V and  $-1.6$  V vs. Ag/AgCl (with saturated KCl). (C) Adsorption of HMF on Pd.

increase for the portions of by-products is even a little more than the decrease for the portions of BHMf. This led to the BHMf SE decreasing more significantly over the Pd<sup>2+</sup> loading of 25 mg/mL. Thus, these results demonstrate that the 15 mg/mL Pd<sup>2+</sup> loading is optimum for this reaction.

We also tried ECH of HMF in different electrolytes over the optimized Pd/GF catalyst (15Pd/GF), and these results are summarized in Figure 3B. Initially, the ECH of HMF was conducted in NaCl, NaClO<sub>4</sub>, and Na<sub>2</sub>SO<sub>4</sub> with a concentration of 0.2 M; the pH of the three solutions with electrolytes is consistent (pH: 4.52~4.61) measured by pH meter (Ohaus STARTER3100). A higher FE and SE of BHMf was achieved in NaClO<sub>4</sub> than the others. It is reported that SO<sub>4</sub><sup>2-</sup> decreases the activity of Pd surfaces due to its strong adsorption at active sites.<sup>45</sup> Cl<sup>-</sup> shows a general adsorption on all types of active sites, whereas ClO<sub>4</sub><sup>-</sup> and SO<sub>4</sub><sup>2-</sup> show adsorption on specific active sites.<sup>46</sup> ClO<sub>4</sub><sup>-</sup> is the optimal anion due to its weak adsorption on Pd catalyst active sites. The different current densities for the ECH of HMF are shown in Figure 3C. At a current density of 50 mA cm<sup>-2</sup>, the highest FE of 72% and SE of 97% were achieved. This is possibly because increasing the current density can accelerate the transfer rate of electrons between the electrode and HMF so that the hydrogenation of HMF is accelerated. However, when the current density increases to a certain value, the catalytic performance decreases with the increase of the current density, due to stronger competing HER and other by-products generation. We found the current density of 100 mA cm<sup>-2</sup> delivers balanced FE and productivity. Moreover, we conducted ECH of HMF at 50 mA cm<sup>-2</sup> for a 2-h continuous experiment (Figure 3D). Up to 1.5 h, FE was maintained at 68%~71%, whereas FE became 62% after 2 h. Meanwhile, SE remained nearly 100% during the continuous reaction. The conversion of HMF (Figure S9) reached the value of 86% at a current density of 50 mA cm<sup>-2</sup> after a 2-h continuous ECH of HMF.

Here in our work, we pursued the superior productivity to the target value-added BHMf. We find the productivity is actually proportional to the partial current density to target product, which is FE multiplied by the total current density (supplemental information). Therefore, we need to run ECH experiments at large current densities, and simultaneously maintain the FE to target product high. Large current densities require high potentials (here more negative), but high potentials lead to stronger competing HER and cause FE to decrease. So, it is of crucial importance to balance the current density and FE, to optimize the partial current density. We designed our ECH system to unite contradictory current density and FE and achieved superior partial current density, i.e., productivity (Table S1).

HMF comprises a reactive C=O and an unsaturated furan ring; however, the bond energy of C=C in the furan ring is lower than that of C=O, so that the hydrogenation of the C=C group should be preferential as opposed to that of the C=O group.<sup>47-49</sup> Intuitively, the ECH of HMF should not preferentially lead to BHMf. We hypothesize it is due to the tilted geometry of HMF molecule adsorbed on Pd surface via carbonyl group, leading to selective production of BHMf. To test the hypothesis and get a deep understanding of the

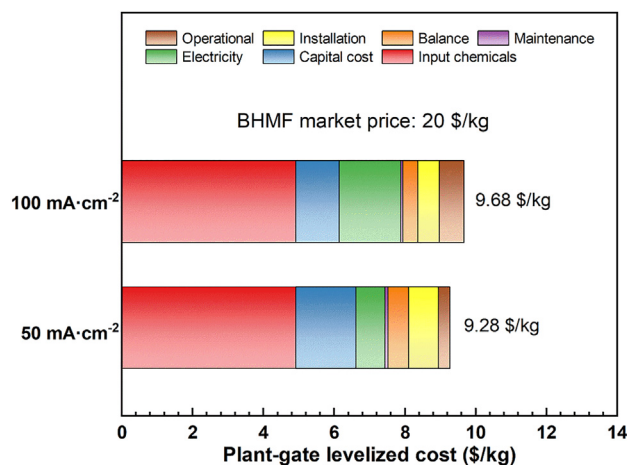


**Figure 5. Preliminary TEA evaluation**

Breakdown of cost on Pd/GF catalyst at a current density of 50 mA cm<sup>-2</sup> and 100 mA cm<sup>-2</sup>; plant-gate leveled cost of BHMf was calculated by a preliminary TEA.

reaction mechanism, we monitored the ECH of HMF on the catalyst surface by *in situ* IRRAS (Figure 4A). As shown in Figure 4B, starting at -0.2 V vs. Ag/AgCl, the growing downward band at 1,690 cm<sup>-1</sup> (C=O)<sup>50,51</sup> is attributed to the disappearance of side-chain carbonyl group (C=O) adsorbed on Pd electrode because of ECH of HMF to BHMf.<sup>52</sup> Meanwhile, the growing upward band centered at 1,080 cm<sup>-1</sup> (C-OH vibration)<sup>53</sup> is attributed to the appearance of new C-OH transformed from hydrogen addition to carbonyl group (C=O). No signal related to the evolution of furan ring is found always up to -1.6 V (vs. Ag/AgCl), indicating that ECH selectively occurs at carbonyl group instead of furan ring, in line with electrochemical experimental results. Thus, IRRAS reveals the ECH reaction pathway to BHMf: HMF molecule is adsorbed on the Pd surface with tilted geometry via carbonyl group, and hydrogen attacks the carbonyl group to form BHMf and then desorbs from Pd surface into the solvent.<sup>54</sup> It shows that Pd/GF electrode catalyzes the ECH reaction in a wide potential range starting at a positive overpotential vs. RHE (-0.2 V vs. Ag/AgCl), indicating that ECH of HMF preferentially occurs over the competing HER. The evolution of infrared spectra proves selective hydrogenation of side-chain carbonyl group instead of C=C in the unsaturated furan ring, which is determined by the tilted geometry of the adsorbed HMF molecule on Pd/GF (Figure 4C). This finding agrees with a recent study about TCH of furfural molecule on Pd.<sup>55</sup> Combining preferential ECH over HER and high SE to the desired product BHMf, IRRAS experiment well explains the resulting high FEs. Owing to the resulting high FEs, larger current densities are accessible, leading to a balanced performance and superior productivity via our ECH system.

### Techno-economic analysis

We performed a preliminary TEA for ECH of HMF to estimate the plant-gate leveled cost of BHMf in an H-cell system (see details in the supplemental information text and Figure S10). The plant-gate leveled cost of BHMf mainly attributes to its FE and current density. In this work, we have achieved an average FE of 72% for BHMf at a current density of 50 mA cm<sup>-2</sup>, and the corresponding TEA result revealed that the plant-gate leveled cost of ECH technology for BHMf is about \$9.28 per kg, profitable compared with its market price of \$20 per kg (Figure 5). In the case of 100 mA cm<sup>-2</sup>, TEA results indicate that the plant-gate leveled cost is ~\$9.68 per kg, a slight increase compared with 50 mA cm<sup>-2</sup>. However, the productivity is enhanced significantly, implying more profits in a unit period for larger current densities.

The electricity price that we used here is 14.04 c/kWh, which is double the US industrial electricity price of 7.02 c/kWh in 2022. Furthermore, the price of renewable electricity is only 3.3 c/kWh for the generation cost of onshore wind electricity from the report of International Renewable Energy Agency's report. What is more, there is still a downward trend for the prices of renewable electricity in the near future accompanying increasingly available renewable electricity. Also, the separation cost is assumed to be 20% of the total electricity cost.<sup>56</sup> The separated solvent is assumed to be recyclable. Therefore, the electricity cost in TEA will be reduced significantly if we replace the electricity cost with renewable electricity.

### Conclusions

In summary, we report an FE of 72%, SE of 97%, and a current density of 50 mA cm<sup>-2</sup> over a Pd/GF catalyst toward a value-added BHMf by ECH of HMF. The record-high productivity of 0.923 mmol cm<sup>-2</sup>·h<sup>-1</sup> at a current density of 100 mA cm<sup>-2</sup> is highlighted in contrast to previous studies. *In situ* IRRAS results elaborate the ECH reaction mechanism and explain the high SE and FEs. A preliminary TEA indicates that our ECH system has the techno-economic feasibility to upgrade HMF to BHMf. This work demonstrates a promising strategy to electrocatalytic upgrade of lignocellulose-derived HMF to value-added chemicals ideally without any CO<sub>2</sub> emission.

**STAR★METHODS**

Detailed methods are provided in the online version of this paper and include the following:

- **KEY RESOURCES TABLE**
- **RESOURCE AVAILABILITY**
  - Lead contact
  - Materials availability
  - Data and code availability
- **METHOD DETAILS**
  - General information
  - Catalyst preparation
  - Catalyst characterization
  - General procedure for the electrocatalytic hydrogenation
  - Product analysis

**SUPPLEMENTAL INFORMATION**

Supplemental information can be found online at <https://doi.org/10.1016/j.isci.2023.108003>.

**ACKNOWLEDGMENTS**

We acknowledge support from the Natural Science Foundation of China (21972096 and 22179086) and the Shenzhen Science and Technology Program (JCYJ20190808150615285).

**AUTHOR CONTRIBUTIONS**

W.Z., Y.Z., and D.Z. conceived the project. D.Z., L.G., and W.Z. designed the experiments. D.Z. and L.G. designed the synthesis of the catalysts and performed the electrochemical measurement. D.Z. designed product analysis by HPLC. W.Z. conducted the in-situ infrared reflection-absorption spectroscopy analysis of the reaction. D.Z. and L.G. wrote the manuscript. All authors commented on the manuscript.

**DECLARATION OF INTERESTS**

The authors declare no competing interests.

**INCLUSION AND DIVERSITY**

We support inclusive, diverse, and equitable conduct of research.

Received: May 8, 2023

Revised: May 28, 2023

Accepted: September 18, 2023

Published: September 23, 2023

**REFERENCES**

1. Alonso, D.M., Bond, J.Q., and Dumesic, J.A. (2010). Catalytic conversion of biomass to biofuels. *Green Chem.* 12, 1493–1513. <https://doi.org/10.1039/c004654j>.
2. Bozell, J.J., and Petersen, G.R. (2010). Technology development for the production of biobased products from biorefinery carbohydrates—the US Department of Energy's "Top 10" revisited. *Green Chem.* 12, 539–554. <https://doi.org/10.1039/b922014c>.
3. Gallezot, P. (2012). Conversion of biomass to selected chemical products. *Chem. Soc. Rev.* 41, 1538–1558. <https://doi.org/10.1039/c1cs15147a>.
4. Chen, H., Peng, T., Liang, B., Zhang, D., Lian, G., Yang, C., Zhang, Y., and Zhao, W. (2022). Efficient electrocatalytic hydrogenation of cinnamaldehyde to value-added chemicals. *Green Chem.* 24, 3655–3661. <https://doi.org/10.1039/d1gc04777a>.
5. Lam, C.H., Deng, W., Lang, L., Jin, X., Hu, X., and Wang, Y. (2020). Minireview on Bio-Oil Upgrading via Electrocatalytic Hydrogenation: Connecting Biofuel Production with Renewable Power. *Energy Fuels* 34, 7915–7928. <https://doi.org/10.1021/acs.energyfuels.0c01380>.
6. Bond, J.Q., Upadhye, A.A., Olcay, H., Tompsett, G.A., Jae, J., Xing, R., Alonso, D.M., Wang, D., Zhang, T., Kumar, R., et al. (2014). Production of renewable jet fuel range alkanes and commodity chemicals from integrated catalytic processing of biomass. *Energy Environ. Sci.* 7, 1500–1523. <https://doi.org/10.1039/c3ee43846e>.
7. Liao, Y., Koelewijn, S.F., Van den Bossche, G., Van Aelst, J., Van den Bosch, S., Renders, T., Navare, K., Nicolai, T., Van Aelst, K., Maesen, M., et al. (2020). A sustainable wood biorefinery for low-carbon footprint chemicals production. *Science* 367, 1385–1390.
8. Sanderson, K. (2011). Lignocellulose: A chewy problem. *Nature* 474, S12–S14.
9. Peng, T., Zhuang, T., Yan, Y., Qian, J., Dick, G.R., Behaghel de Bueren, J., Hung, S.F., Zhang, Y., Wang, Z., Wicks, J., et al. (2021). Ternary Alloys Enable Efficient Production of Methoxylated Chemicals via Selective Electrocatalytic Hydrogenation of Lignin Monomers. *J. Am. Chem. Soc.* 143, 17226–17235. <https://doi.org/10.1021/jacs.1c08348>.
10. Wan, J., Zeng, Y., Wang, M., Dong, B., Xu, Z., Kumar, M., Zhang, Y., and Zhao, W. (2022). Electrocatalytic hydrogenation of lignin monomer to methoxy-cyclohexanes with high faradaic efficiency. *Green Chem.* 116, 142–150. <https://doi.org/10.1039/d1gc03523a>.
11. Yang, C., Chen, H., Peng, T., Liang, B., Zhang, Y., and Zhao, W. (2021). Lignin valorization

- toward value-added chemicals and fuels via electrocatalysis: A perspective. *Chinese J. Catal.* **42**, 1831–1842. [https://doi.org/10.1016/s1872-2067\(21\)63839-1](https://doi.org/10.1016/s1872-2067(21)63839-1).
12. Takagaki, A., Nishimura, S., and Ebitani, K. (2012). Catalytic Transformations of Biomass-Derived Materials into Value-Added Chemicals. *Catal. Surv. Asia* **16**, 164–182. <https://doi.org/10.1007/s10563-012-9142-3>.
  13. van Putten, R.J., van der Waal, J.C., de Jong, E., Rasrendra, C.B., Heeres, H.J., and de Vries, J.G. (2013). Hydroxymethylfurfural, a versatile platform chemical made from renewable resources. *Chem. Rev.* **113**, 1499–1597. <https://doi.org/10.1021/cr300182k>.
  14. Rosatella, A.A., Simeonov, S.P., Frade, R.F.M., and Afonso, C.A.M. (2011). 5-Hydroxymethylfurfural (HMF) as a building block platform: Biological properties, synthesis and synthetic applications. *Green Chem.* **13**, 754–793. <https://doi.org/10.1039/c0gc00401d>.
  15. Shanks, B.H., and Keeling, P.L. (2017). Bioprivileged molecules: creating value from biomass. *Green Chem.* **19**, 3177–3185. <https://doi.org/10.1039/c7gc00296c>.
  16. Rao, K.T.V., Hu, Y., Yuan, Z., Zhang, Y., and Xu, C.C. (2021). Green synthesis of heterogeneous copper-alumina catalyst for selective hydrogenation of pure and biomass-derived 5-hydroxymethylfurfural to 2,5-bis(hydroxymethyl)furan. *Appl. Catal. A-Gen.* **609**, 117892. <https://doi.org/10.1016/j.apcata.2020.117892>.
  17. Aricò, F. (2021). Synthetic approaches to 2,5-bis(hydroxymethyl)furan (BHMF): a stable bio-based diol. *Pure Appl. Chem.* **93**, 551–560. <https://doi.org/10.1515/pac-2021-0117>.
  18. Op de Beeck, B., Dusselier, M., Geboers, J., Holsbeek, J., Morrè, E., Oswald, S., Giebelers, L., and Sels, B.F. (2015). Direct catalytic conversion of cellulose to liquid straight-chain alkanes. *Energy Environ. Sci.* **8**, 230–240. <https://doi.org/10.1039/c4ee01523a>.
  19. Alamillo, R., Tucker, M., Chia, M., Pagán-Torres, Y., and Dumesic, J. (2012). The selective hydrogenation of biomass-derived 5-hydroxymethylfurfural using heterogeneous catalysts. *Green Chem.* **14**, 1413–1419. <https://doi.org/10.1039/c2gc35039d>.
  20. Ohyama, J., Esaki, A., Yamamoto, Y., Arai, S., and Satsuma, A. (2013). Selective hydrogenation of 2-hydroxymethyl-5-furfural to 2,5-bis(hydroxymethyl)furan over gold sub-nano clusters. *RSC Adv.* **3**, 1033–1036. <https://doi.org/10.1039/c2ra22190j>.
  21. Ohyama, J., Hayashi, Y., Ueda, K., Yamamoto, Y., Arai, S., and Satsuma, A. (2016). Effect of FeOx Modification of Al<sub>2</sub>O<sub>3</sub> on Its Supported Au Catalyst for Hydrogenation of 5-Hydroxymethylfurfural. *J. Phys. Chem. C* **120**, 15129–15136. <https://doi.org/10.1021/acs.jpcc.6b01542>.
  22. Cai, H., Li, C., Wang, A., and Zhang, T. (2014). Biomass into chemicals: One-pot production of furan-based diols from carbohydrates via tandem reactions. *Catal. Today* **234**, 59–65. <https://doi.org/10.1016/j.cattod.2014.02.029>.
  23. Tamura, M., Tokonomi, K., Nakagawa, Y., and Tomishige, K. (2013). Rapid synthesis of unsaturated alcohols under mild conditions by highly selective hydrogenation. *Chem. Commun. (Camb)* **49**, 7034–7036. <https://doi.org/10.1039/c3cc41526k>.
  24. Ratvey, G., Solanki, B.S., Kamble, S.P., and Rode, C.V. (2022). Highly Efficient Chemoselective Hydrogenation of 5-HMF to BHMF over Reusable Bimetallic Pd-Ir/C Catalyst. *ChemistrySelect* **7**, e202200456. <https://doi.org/10.1002/slct.202200456>.
  25. Akhade, S.A., Singh, N., Gutiérrez, O.Y., Lopez-Ruiz, J., Wang, H., Holladay, J.D., Liu, Y., Karkamkar, A., Weber, R.S., Padmaperuma, A.B., et al. (2020). Electrocatalytic Hydrogenation of Biomass-Derived Organics: A Review. *Chem. Rev.* **120**, 11370–11419. <https://doi.org/10.1021/acs.chemrev.0c00158>.
  26. Wijaya, Y.P., Smith, K.J., Kim, C.S., and Gyenge, E.L. (2020). Electrocatalytic hydrogenation and depolymerization pathways for lignin valorization: toward mild synthesis of chemicals and fuels from biomass. *Green Chem.* **22**, 7233–7264. <https://doi.org/10.1039/d0gc02782k>.
  27. Li, K., and Sun, Y. (2018). Electrocatalytic Upgrading of Biomass-Derived Intermediate Compounds to Value-Added Products. *Chemistry* **24**, 18258–18270. <https://doi.org/10.1002/chem.201803319>.
  28. Nilges, P., and Schröder, U. (2013). Electrochemistry for biofuel generation: production of furans by electrocatalytic hydrogenation of furfural. *Energy Environ. Sci.* **6**, 2925–2931. <https://doi.org/10.1039/c3ee41857j>.
  29. Sanghez de Luna, G., Ho, P.H., Loli, A., Ospitali, F., Albonetti, S., Fornasari, G., and Benito, P. (2020). Ag Electrodeposited on Cu Open-Cell Foams for the Selective Electroreduction of 5-Hydroxymethylfurfural. *Chemelectrochem* **7**, 1238–1247. <https://doi.org/10.1002/celec.201902161>.
  30. Chadderdon, X.H., Chadderdon, D.J., Pfennig, T., Shanks, B.H., and Li, W. (2019). Paired electrocatalytic hydrogenation and oxidation of 5-(hydroxymethyl)furfural for efficient production of biomass-derived monomers. *Green Chem.* **21**, 6210–6219. <https://doi.org/10.1039/c9gc02264c>.
  31. Liu, H., Lee, T.-H., Chen, Y., Cochran, E.W., and Li, W. (2021). Paired electrolysis of 5-(hydroxymethyl)furfural in flow cells with a high-performance oxide-derived silver cathode. *Green Chem.* **23**, 5056–5063. <https://doi.org/10.1039/d1gc00988e>.
  32. Zhang, L., Zhang, F., Michel, F.C., and Co, A.C. (2019). Efficient Electrochemical Hydrogenation of 5-Hydroxymethylfurfural to 2,5-Bis(hydroxymethyl)furan on Ag-Displaced Nanotextured Cu Catalysts. *Chemelectrochem* **6**, 4739–4749. <https://doi.org/10.1002/celec.201900640>.
  33. Ji, K., Xu, M., Xu, S.M., Wang, Y., Ge, R., Hu, X., Sun, X., and Duan, H. (2022). Electrocatalytic Hydrogenation of 5-Hydroxymethylfurfural Promoted by a Ru1 Cu Single-Atom Alloy Catalyst. *Angew. Chem. Int. Ed. Engl.* **61**, e202209849. <https://doi.org/10.1021/jp305166k>.
  34. Kibis, L.S., Stadnichenko, A.I., Koscheev, S.V., Zaikovskii, V.I., and Boronin, A.I. (2012). Highly Oxidized Palladium Nanoparticles Comprising Pd<sup>4+</sup> Species: Spectroscopic and Structural Aspects, Thermal Stability, and Reactivity. *J. Phys. Chem. C* **116**, 19342–19348. <https://doi.org/10.1021/jp305166k>.
  35. Tressaud, A., Khairoun, S., Touhara, H., and Watanabe, N. (1986). X-Ray Photoelectron Spectroscopy of Palladium Fluorides. *Z. für Anorg. Allg. Chem.* **540**, 291–299.
  36. Militello, M.C., and Simko, S.J. (1994). Palladium Oxide (PdO) by XPS. *Surf. Sci. Spectra* **3**, 395–401.
  37. Zhao, Y., Lin, Y., Miao, B., Ding, Y., Jin, P., and Chen, Y. (2022). One-dimensional Rhodium-nickel Alloy Assemblies with Nanodendrite Subunits for Alkaline Methanol Oxidation. *Chin. J. Struct. Chem.* **41**, 2204040–2204045. <https://doi.org/10.14102/j.cnki.0254-5861.2022-0019>.
  38. Wang, T.J., Jiang, Y.C., He, J.W., Li, F.M., Ding, Y., Chen, P., and Chen, Y. (2022). Porous palladium phosphide nanotubes for formic acid electrooxidation. *Carbon Energy* **4**, 283–293. <https://doi.org/10.1002/cey2.170>.
  39. Ding, Y., Miao, B.-Q., Liu, Y.-C., Hou, N., Yang, Y., Jin, P.-J., Yin, S.-B., and Chen, Y. (2022). Rhodium-Cobalt Alloy Nanotubes Toward Methanol Oxidation Reaction. *Small Structures* **3**. <https://doi.org/10.1002/ssstr.202200046>.
  40. Ilkiv, B., Petrovska, S., Sergiienko, R., Foya, O., Ilkiv, O., Shibata, E., Nakamura, T., and Zaulychnyy, Y. (2014). Electronic Structure of Hollow Graphitic Carbon Nanoparticles Fabricated from Acetylene Carbon Black. Fuller. Nanotub. Carbon Nanostructures **23**, 449–454. <https://doi.org/10.1080/1536383x.2014.885957>.
  41. Gogoi, P., Kanna, N., Begum, P., Deka, R.C., Satyanarayana, C.V.V., and Raja, T. (2019). Controlling and Stabilization of Ru Nanoparticles by Tuning the Nitrogen Content of the Support for Enhanced H<sub>2</sub> Production through Aqueous-Phase Reforming of Glycerol. *ACS Catal.* **10**, 2489–2507. <https://doi.org/10.1021/acscatal.9b04063>.
  42. Budarin, V.L., Clark, J.H., Luque, R., Macquarrie, D.J., and White, R.J. (2008). Palladium nanoparticles on polysaccharide-derived mesoporous materials and their catalytic performance in C–C coupling reactions. *Green Chem.* **10**, 382–387. <https://doi.org/10.1039/b715508e>.
  43. Fang, L.I., Tao, Q., Li, M.f., Liao, L.w., Chen, D., and Chen, Y.x. (2010). Determination of the Real Surface Area of Palladium Electrode. *Chi. J. Chem. Phys.* **23**, 543–548. <https://doi.org/10.1088/1674-0068/23/05/543-548>.
  44. Cuesta, A., Kibler, L., and Kolb, D.M. (1999). A method to prepare single crystal electrodes of reactive metals: application to Pd(hkl). *J. Electroanal. Chem.* **466**, 165–168.
  45. Sharma, H.N., Sharma, V., Mhadeshwar, A.B., and Ramprasad, R. (2015). Why Pt Survives but Pd Suffers From SO<sub>x</sub> Poisoning? *J. Phys. Chem. Lett.* **6**, 1140–1148. <https://doi.org/10.1021/jz5027147>.
  46. Dalavoy, T., Jackson, J., Swain, G., Miller, D., Li, J., and Lipkowsky, J. (2007). Mild electrocatalytic hydrogenation of lactic acid to lactaldehyde and propylene glycol. *J. Catal.* **246**, 15–28. <https://doi.org/10.1016/j.jcat.2006.11.009>.
  47. Gallezot, P., and Richard, D. (1998). Selective Hydrogenation of  $\alpha,\beta$ -Unsaturated Aldehydes. *Catal. Rev. Sci. Eng.* **40**, 81–126. <https://doi.org/10.1080/01614949808007106>.
  48. Luneau, M., Lim, J.S., Patel, D.A., Sykes, E.C.H., Friend, C.M., and Sautet, P. (2020). Guidelines to Achieving High Selectivity for the Hydrogenation of  $\alpha,\beta$ -Unsaturated Aldehydes with Bimetallic and Dilute Alloy Catalysts: A Review. *Chem. Rev.* **120**, 12834–12872. <https://doi.org/10.1021/acs.chemrev.0c00582>.
  49. Luneau, M., Lim, J.S., Patel, D.A., Sykes, E.C.H., Friend, C.M., and Sautet, P. (2020). Guidelines to achieving high selectivity for the hydrogenation of  $\alpha,\beta$ -unsaturated aldehydes with bimetallic and dilute alloy catalysts - A review. *Chem. Rev.* **120**, 12834–12872.

50. Araujo-Andrade, C., Gómez-Zavaglia, A., Reva, I.D., and Fausto, R. (2012). Conformers, infrared spectrum and UV-induced photochemistry of matrix-isolated furfuryl alcohol. *J. Phys. Chem. A* *116*, 2352–2365. <https://doi.org/10.1021/jp212169b>.
51. Zhang, K., Meng, Q., Wu, H., He, M., and Han, B. (2022). Selective Hydrogenolysis of 5-Hydroxymethylfurfural into 2,5-Dimethylfuran under Mild Conditions Using Pd/MOF-808. *ACS Sustain. Chem. Eng.* *10*, 10286–10293. <https://doi.org/10.1021/acssuschemeng.2c02393>.
52. Edwards, E.R., Oishi, S.S., and Botelho, E.C. (2018). Analysis of chemical polymerization between functionalized MWCNT and poly(furfuryl alcohol) composite. *Polímeros* *28*, 15–22. <https://doi.org/10.1590/0104-1428.07016>.
53. O'Driscoll, Á., Curtin, T., Hernández, W.Y., Van Der Voort, P., and Leahy, J.J. (2016). Hydrogenation of Furfural with a Pt–Sn Catalyst: The Suitability to Sustainable Industrial Application. *Org. Process Res. Dev.* *20*, 1917–1929. <https://doi.org/10.1021/acs.oprd.6b00228>.
54. Vorotnikov, V., Mpourmpakis, G., and Vlachos, D.G. (2012). DFT Study of Furfural Conversion to Furan, Furfuryl Alcohol, and 2-Methylfuran on Pd(111). *ACS Catal.* *2*, 2496–2504. <https://doi.org/10.1021/cs300395a>.
55. Yu, I.K.M., Deng, F., Chen, X., Cheng, G., Liu, Y., Zhang, W., and Lercher, J.A. (2022). Impact of hydronium ions on the Pd-catalyzed furfural hydrogenation. *Nat. Commun.* *13*, 7154. <https://doi.org/10.1038/s41467-022-34608-8>.
56. Jouny, M., Luc, W., and Jiao, F. (2018). General Techno-Economic Analysis of CO<sub>2</sub> Electrolysis Systems. *Ind. Eng. Chem. Res.* *57*, 2165–2177. <https://doi.org/10.1021/acs.iecr.7b03514>.
57. Anibal, J., and Xu, B. (2020). Electroreductive C–C Coupling of Furfural and Benzaldehyde on Cu and Pb Surfaces. *ACS Catal.* *10*, 11643–11653. <https://doi.org/10.1021/acscatal.0c03110>.

## STAR★METHODS

### KEY RESOURCES TABLE

REAGENT or RESOURCE	SOURCE	IDENTIFIER
Chemicals, peptides, and recombinant proteins		
5-Hydromethylfurfural (HMF, 98%)	Innochem	CasNo: 67-47-0
Palladium (II) chloride (PdCl <sub>2</sub> , Pd 59–60%)	Innochem	CasNo: 7647-10-1
5-Methyl-2-furanmethanol (HMMF, 95+%)	Innochem	CasNo: 3857-25-8
Ammonium formate (HCOONH <sub>4</sub> , 99%)	Innochem	CasNo: 540-69-2
Acetonitrile (CH <sub>3</sub> CN, >99.9%)	Innochem	CasNo: 75-05-8
Sodium sulfate (Na <sub>2</sub> SO <sub>4</sub> , 99%)	Innochem	CasNo: 7757-82-6
5-Methylfurfural (MF, 98%)	Aladin	CasNo: 620-02-0
Sodium perchlorate (NaClO <sub>4</sub> , ≥ 98.0%)	Aladin	CasNo: 7601-89-0
2, 5-Furandimethanol (BHMF, ≥ 98.0%)	Alfa Aesar	CasNo: 1883-75-6
Potassium hydroxide (KOH, 98%)	Macklin	CasNo: 1310-58-3
Hydrochloric acid (HCl, 36%~38%)	Guangzhou Chemical Reagent Factory	CasNo:7647-01-0

### RESOURCE AVAILABILITY

#### Lead contact

Further information and requests for resources should be directed to and will be fulfilled by the lead contact, Wei Zhao ([weizhao@szu.edu.cn](mailto:weizhao@szu.edu.cn)).

#### Materials availability

All reagents were purchased from commercial sources and used without purification unless otherwise mentioned. All materials generated in this study are available from the [lead contact](#) without restriction.

#### Data and code availability

- Data reported in this paper will be shared by the [lead contact](#) upon request.
- This paper does not report original code.
- Any additional information required to reanalyze the data reported in this paper is available from the [lead contact](#) upon request.

### METHOD DETAILS

#### General information

The equipment for valuation of electrocatalytic hydrogenation (ECH) was a H-cell vessel with a magnetic stirring. Products were qualitatively and quantitatively analyzed by the Agilent 1260 high performance liquid chromatography (HPLC) equipped with Poroshell 120 SB-Aq column and a variable wavelength detector (VWD). The faradaic efficiency, selectivity, conversion and productivity of products were calculated with internal standard method. The commercial standard samples and the Agilent LC1290-6550 liquid chromatography-mass spectrometry (LC-MS) were used to confirm the structure of product.

#### Catalyst preparation

Graphite felt (GF, 1 cm × 1.5 cm) was slightly extruded to exhaust bubble with 0.5 M hydrochloric acid in advance and then dried for standby. First, we prepared 0.025 g PdCl<sub>2</sub> soluble in 0.5 M hydrochloric acid of 1 mL (corresponding to 15 mg/mL Pd<sup>2+</sup> loading in [Figure 4A](#)). After heating for 5 minutes at 70°C, a homogeneous aqueous solution was obtained. Then inject the solution of 100 uL onto the GF (1 cm × 1 cm) evenly with a pipette and take it to dry. Repeat the above steps until all solution was injected into the GF uniformly and finally dried. Finally, the GF loading the precursors was heated from 30°C to 500°C under an argon flow of 50 mL/min in a tubular furnace for 47 min at a heating rate of 10°C/min and then maintained at 500°C for 1 h, finally cooled down to room temperature. This catalyst was denoted as the Pd/GF catalyst.

#### Catalyst characterization

The metal content was analyzed with an inductively coupled plasma mass spectroscopy (ICP-MS, Agilent 720S). The morphological analysis and elemental distribution were studied by a scanning electron microscope (SEM, Thermo Scientific Apreo 2C) equipped with an energy

dispersive spectroscopy detector. The morphology of Pd/GF catalyst was carried out using a transmission electron microscope (TEM, Talos F200S G2). X-ray diffraction (XRD, Copper target, Rigaku Smartlab) and X-ray photoelectron spectroscopy (XPS, Thermo Scientific K-Alpha<sup>+</sup>) were employed to characterize the crystal structure and elemental state of Pd/GF catalyst. *In-situ* infrared reflection–absorption spectroscopy (IRRAS, Thermo Scientific Nicolet is50 FT-IR), equipped with an A-type mercuric cadmium telluride (MCT) detector, was employed to investigate the mechanism of the ECH reaction.

### General procedure for the electrocatalytic hydrogenation

The ECH of HMF was performed in a H-cell vessel with a magnetic stirring. A saturated Ag/AgCl electrode (with saturated KCl) was used as the reference electrode, and a Pt mesh was used as the counter electrode. The two chambers were separated by a bipolar membrane. The typical step is as follows: 30 mL cathodic solution (50 mM HMF, 0.2 M NaClO<sub>4</sub>, pH 4.52) is added to the cathode chamber, and 30 mL anodic solution (1 M KOH) is added to the anode chamber. Clip the Pd/GF catalyst with an electrode clamp and make the exposed catalyst area 1 × 1 cm<sup>2</sup>. The working electrode and Ag/AgCl electrode are on the side of the cathode chamber, while the Pt electrode is on the side of the anode chamber. Adjust the position of the three electrodes on the cover so that they are in a straight line and the three electrodes are parallel to the bipolar membrane. After adjusting the position of the three electrodes, the electrochemical workstation (CHI760E) is utilized for the chronopotentiometry test at room temperature. Especially, the stability test for ECH of HMF was performed in the flow cell system equipped with a IrO<sub>2</sub> contact electrode. Beforehand, the Pd/GF catalyst was reduced for 30 min with both chambers filled with 0.2 M Na<sub>2</sub>SO<sub>4</sub> solutions. When the reaction is completed, the cathodic solution is transferred to tumbler and the obtained products are detected by the Agilent HPLC.

### Product analysis

Products as shown in Figure S1 were qualitatively and quantitatively analyzed by high performance liquid chromatography (HPLC, Agilent 1260 Infinity Series) equipped with a variable wavelength detector (VWD) at 230 nm. The column (InfinityLab Poroshell 120 SB-Aq, 4.6 × 250 mm) was operated at 25°C with a binary gradient pumping method containing CH<sub>3</sub>CN and H<sub>2</sub>O with 10 mM ammonium formate at a flow rate of 1 mL/min. The CH<sub>3</sub>CN fraction was kept at 10% (v/v) until 6.50 minute and then increased from the initial 10% (v/v) to 28% over 6.5 ~ 9 minute, then was increased from 28% to 60% over 15 ~ 18 minute. BHMF and HMF were eluted around 4.25 and 5.34 minute, respectively. The HMF dimer, BHH, was eluted at a retention time (4.11 minute). Other products including HMMF and MF were eluted at 8.57 and 10.19 minutes, respectively. The standard samples of HMF and ECH products were purchased for qualitative and quantitative analysis, except for BHH. Qualitative analysis of BHH (Figure S2) was conducted by liquid chromatography-mass spectrometry (LC-MS, Agilent LC1290-6550 QTOF). Since a commercial BHH sample was not available, the quantitative calibration was estimated as twice that of BHMF, the same method applied in the previous literature.<sup>57</sup> Guaiacol was selected as an appropriate internal standard for the quantitative analysis. The faradaic efficiency, the selectivity and productivity of hydrogenation products and conversion of HMF were calculated based on the following equations:

$$j = \frac{I}{A}$$

$$\text{Faradaic efficiency (FE)} = \frac{n_i * Z_i * F}{I * t} \times 100\%$$

$$\text{Selectivity (SE)} = \frac{n_i}{\sum n_i} \times 100\%$$

$$\text{Conversion} = \frac{\text{moles of HMF consumed}}{\text{initial moles of HMF}} \times 100\%$$

$$\text{Productivity} = \frac{n_i}{\text{area of GF} * t}$$

where  $j$  is current density;  $I$  is current;  $A$  is area of catalyst;  $n_i$  is the number of mole of product  $i$  formed;  $Z_i$  is the number of electrons transferred for the corresponding reduction process from HMF to product  $i$ ,  $Z = 2$  for BHMF, MF, BHH, and H<sub>2</sub>,  $Z = 4$  for HMMF;  $F$  is the Faraday constant (96485.333 C/mol). Here, area of GF in the productivity formula represents the geometrical area of Pd/GF electrode as 1 cm<sup>2</sup>.